A Study of the Sensitivity of Biomechanical Models of the Spine for Scoliosis Brace Design

Christos Koutras[1,*], Jesús Pérez[1], Kateryna Kardash[1], Miguel A. Otaduy[1]

Universidad Rey Juan Carlos, Madrid, 28933, Spain

Abstract

Background and Objective: The development of biomechanical models of the torso and the spine opens the door to computational solutions for the design of braces for adolescent idiopathic scoliosis. However, the design of such biomechanical models faces several unknowns, such as the correct identification of relevant mechanical elements, or the required accuracy of model parameters. The objective of this study was to design a methodology for the identification of the aforementioned elements, with the purpose of creating personalized models suited for patient-specific brace design and the definition of parameter estimation criteria.

Methods: We have developed a comprehensive model of the torso, including spine, ribcage and soft tissue, and we have developed computational tools for the analysis of the model parameters. With these tools, we perform an analysis of the model under typical loading conditions of scoliosis braces.

Results: We present a complete sensitivity analysis of the model's mechanical parameters and a comparison between a reference healthy subject and a subject suffering from scoliosis. Furthermore, we make a direct connection between error bounds on the deformation and tolerances for parameter estimation, which can guide the personalization of the model.

Conclusions: Not surprisingly, the stiffness parameters that govern the lateral deformation of the spine in the frontal plane are some of the most relevant parameters, and require careful modeling. More surprisingly, their relevance is on par with the correct parameterization of the soft tissue of the torso. For scoliosis patients, but not for healthy subjects, we observe that the axial rotation of the spine also requires careful modeling.

Keywords: Computational biomechanics, sensitivity analysis, computer model of torso, scoliosis

1. Introduction

Scoliosis problems of moderate degree on adolescents are typically treated using orthotic brace structures that push the spine. Scoliosis braces are designed in a variety of shapes and procedures. Most design methods rely to date on physical experimentation and prototyping, although computational strategies have been moderately studied; see [16, 52] for some comparisons. Wider adoption of computational methods for the design of scoliosis braces suffers an important challenge: they require a personalized model of the patient's torso biomechanics.

1.1. Background / Spine Modeling and Parameter Estimation

Designing a personalized biomechanical model entails two tasks: fitting the morphology and connections of anatomical elements to those of the patient, and parameterizing the mechanical models to match the response of the patient's body. Biomechanical modeling of the spine has received a lot of attention, with popular approaches largely divided into two categories. One category follows the Finite Element Method (FEM); please see [53] for a survey of methods. Many FEM models have been developed for the lumbar [20, 22, 55], thoracic [3, 4] or the cervical spine [28]. Furthermore, Dicko et al. [19] developed a hybrid lumbar spine model containing rigid bodies, FEM and contact mechanics, while Clin et al. [14] developed a novel method to include gravitational forces in an FE model. While these methods are potentially accurate, they require careful estimation of model parameters for personalized design applications.

FE models of the torso have been coupled to brace models and patient geometry for personalized brace design in the context of adolescent idiopathic scoliosis [23, 31, 37]. Some studies include the evaluation of the effectiveness of these techniques on large cohorts of patients [17, 25, 51].

Another category of approaches uses a simpler but more efficient solution based on multi-body models. De Zee et al. [18] made a generic detailed rigid-body model of the

*Corresponding author

Email addresses: christos.koutras@urjc.es (Christos Koutras), jesus.perez@urjc.es (Jesús Pérez), kateryna.kardash@urjc.es (Kateryna Kardash), miguel.otaduy@urjc.es (Miguel A. Otaduy)

lumbar spine. Bayoglu et al. [6] developed a multi-body muscoloskeletal model of the human spine in order to study the spinal loads. Raabe et al. [43] investigated the jogging biomechanics using a full-body spine model developed in OpenSim, an open-source musculoskeletal simulation software. Naveaux et al. [29] developed biomechanical models based on multi-body dynamics to analyze the effects of implant density and distribution on curve correction and the resulting forces on the vertebrae. Ignasiak et al. [27] predicted the dynamic spinal loading using a multi-body thoracolumbar spine model with articulated rib cage.

In the category of multi-body models, a strong effort has been devoted to finding accurate simplifications of the models and designing parameter estimation techniques. In our design and parameterization of a spine-and-torso model, we borrow insight and design choices from this collection of work.

Panjabi et al. [40] studied the mechanical behavior of the human lumbar and lumbosacral spine as shown by three dimensional load-displacement curves. Panjabi et al. [39] estimated the rotational stiffness coefficients of the thoracic spine from experiments. Bisschop et al. [8] and Panjabi et al. [39] found the translational stiffness coefficients of the thoracic spine through experimental studies. Moroney et al. [36] estimated the load displacement properties of the cervical spine from experiments. Andriacchi et al. [48] estimated the stiffness coefficients of the elastic properties of the rib cage through simulations. Wilke et al. [54] examined the flexibility of every thoracic spinal segment in an in-vitro experiment. Liebsch et al. [32, 33] investigated the kinematic and stiffness properties of the thoracic spine and the rib cage through experimental studies.

Moreover, many studies tried to estimate the mechanical parameters of the soft tissue in the human's body. Choi et al. [10] estimated Young's modulus and Poisson's ratio of soft tissue from indentation using two different-sized indentors in a finite element analysis. Song et al. [47] studied the elasticity of the living abdominal wall in laparoscopic surgery. Hostettler et al. [26] measured the Bulk modulus and volume variation of the liver and the kidneys in vivo. McKee et al. [35] compared the reported values of Young's modulus obtained from indentation and tensile deformations of soft biological tissues.

1.2. Background / Sensitivity Analysis

As discussed above, the biomechanics of the torso and the spine have been thoroughly studied, but hardly from the perspective of their accuracy for the computational design of scoliosis braces. Multiple questions arise in this regard, such as the identification of the anatomical elements that play a relevant role, or the required accuracy of the model parameters. In this work, we study these questions, with the goal of setting guidelines for the design of practical personalized models and the estimation of model parameters. We do this by analyzing the sensitivity of model parameters to guide parameter estimation.

Several previous works also analyzed the sensitivity of various model components. Zander et al. [56] analyzed sensitivity to the position of the intervertebral centers of rotation in upright standing using a musculoskeletal lumbar spine model. Bauer et al. [5] performed sensitivity analysis of intervertebral disc parameters in a multibody-model of the lumbar spine. Senteler et al. [45] analyzed the sensitivity of interverteral joint forces to the center of rotation location. Putzer et al. [41] conducted a sensitivity analysis of lumbar spine loadings to anatomical parameters. Bayoglu et al. [7] analyzed the sensitivity of muscle and intervertebral disc computations against potential errors in modelling muscle attachment sites. Xu et al. [55] conducted a mesh convergence and material sensitivity analysis on a finite element model of healthy lumbar spine. Clin et al. [15] analyzed the sensitivity of brace efficiency to multiple brace designs.

To the best of our knowledge, no prior study analyzed the sensitivity of biomechanical models of the torso and the spine under the loading conditions of scoliosis braces. Our study, on the other hand, is aimed at guiding parameter estimation for the computational design of braces. Furthermore, previous works on sensitivity analysis of spine models often focus on portions of the spine, or model elements of the spine to a degree of complexity beyond our needs. Instead, we apply sensitivity analysis to a comprehensive model of the spine and the torso, including soft tissue, with a degree of complexity suited for scoliosis brace design. Precisely one of our goals is the validation of the components of the model. From the point of view of methodology, we depart from sensitivity analysis approaches based on sampling and statistical tools, and rely instead on local linear analysis and linear algebra tools, as done often in structural design [21, 50]. We extend these tools for the derivation of parameter tolerances based on prescribed bounds on the model's accuracy.

1.3. Contributions

As the first component of our methods (see Section 2), we develop a comprehensive model of the passive biomechanics of the torso, with a focus on the deformation of the thoracolumbar spine. We deform this model using reference loadings that mimic the action of typical scoliosis braces, and we perform a comparative study by applying the model to data from both healthy and pathological subjects.

As the second component of our methods (see Section 3), and to facilitate experimental analysis for a torso model with many degrees of freedom and many mechanical parameters, we design mathematical tools that operate in a linearized regime with respect to equilibrium conditions. In particular, we show how to derive a sensitivity matrix that relates model parameters to the deformed configuration of the torso, subject to implicit static equilibrium constraints. Furthermore, we show how to leverage various linear algebra tools to carry out analysis operations on the sensitivity matrix.

The study of parameter sensitivity allows us to draw important conclusions for the design of personalized biomechanical models in the context of computational brace design. First and foremost, the impact of soft tissue cannot be neglected. Many biomechanical models focus on the musculoskeletal system, but we have found that the required accuracy on the parameters of the soft-tissue model is on par with the stiffness parameters that govern lateral motion of the spine in the frontal plane. In addition, we have found that the axial rotation stiffness of the spine is not relevant for healthy subjects, but it gains relevance for subjects suffering from scoliosis. Finally, we also derive tolerance values for the various model parameters as a function of admissible error bounds on spine deformation.

2. Methods / Biomechanical Model of the Torso

In this section, we describe our biomechanical model of the torso, which represents the main biomechanical elements involved in brace-body interaction. The proposed biomechanical model will be used to predict the change in static spine configuration due to surface forces. More specifically, we want to analyze the sensitivity of the static spine configuration with regard to the various mechanical parameters of the torso. We start this section by providing an overview of the model, with an overall summary of its main ingredients and design choices. The interested reader may then continue with the rest of the section to understand the details of the model, or may jump to the next section to discover how the model is used for sensitivity analysis.

2.1. Overview of the Biomechanical Model

Let us start by identifying the main variables of our model. First, the degrees of freedom (DoFs) $\mathbf{x}$ gather the rigid transformations of bones and the locations of discrete nodes that sample the soft tissue of the torso. Second, the model parameters ξ gather stiffness values of bone joints and parameter values of the soft-tissue model. And third, the boundary conditions $\mathbf{f}_{ext}$ represent external forces applied on the torso, which mimic the interaction produced by scoliosis braces.

The purpose of the biomechanical model is to find the static-equilibrium configuration of the spine and torso, given a set of parameter values and known external forces. The biomechanical model can be interpreted as a function f that maps parameter values ξ and external forces $\mathbf{f}$ to a configuration $\mathbf{x}$ that satisfies static equilibrium. The model can then be summarized as

$$\mathbf{x} = f(\mathbf{f}_{ext}, \xi), \tag{1}$$

To enable sensitivity analysis, we require a biomechanical model that is differentiable with respect to the mechanical parameters. We achieve this by designing the biomechanical model as an unconstrained energy minimization problem, which combines potential energy due to gravity, soft-tissue elastic energy, and skeletal joint energies. Then, given a total energy function E, the model f in (1) can be rewritten as:

$$\mathbf{x} = \arg\min_{\mathbf{x}} E(\mathbf{x}, \xi) - \mathbf{f}_{ext}^T \mathbf{x}. \tag{2}$$

The minimization (2) is satisfied when the net forces on the torso are zero, which corresponds to static equilibrium conditions. With internal forces $\mathbf{f} = -\nabla_{\mathbf{x}} E$, the biomechanical model f is then defined implicitly by the following static equilibrium condition:

$$\mathbf{f}(\mathbf{x}, \xi) + \mathbf{f}_{ext} = 0. \tag{3}$$

We make several design choices to limit the complexity of the model while retaining sufficient accuracy for the problem at hand. In particular, we consider the torso model passive, without muscle activation. We are looking at setting up an accurate model capable of predicting how surface forces produced by a scoliosis brace act on the spine. While the exact instantaneous forces depend on the instantaneous muscle activity, scoliosis braces perform most of their action during periods of little muscle activity. Therefore, we discard muscle activity in our study.

We also decide to model the skeletal structure as a multibody system of rigid bones connected by compliant joints. To satisfy differentiability of the model, we avoid using hard constraints at joints. Specifically, we use a model of anisotropic compliant 6D joint, and we continue this section with a detailed description of this joint model. Next, we discuss the construction of the full articulated body that represents the spine, the rib cage, the sternum, and their connections. We pay particular attention to the choice of default parameters for the different joints, based on previous literature in the field. We continue with a discussion of our soft-tissue model and its connection to the articulated skeleton. We also discuss in detail how we apply boundary conditions. Finally, we describe the details of the static equilibrium formulation that combines all the previous elements.

2.2. 6D Joint Model

Let us consider two bones, a parent p and a child c, defined by their respective translation and rotation, $(\mathbf{x}_p, \mathbf{R}_p)$ and $(\mathbf{x}_c, \mathbf{R}_c)$, as shown in Fig. 1. We consider that all bones have zero rotation in the rest configuration. We place a 6D joint between the pair of bones, i.e., a joint that creates both a force and a torque that counteract the relative motion between the bones. Each joint is located and oriented according to its biomechanical functionality. In Section 2.3 below, we discuss this process for the different types of joints in our model.

The location of a joint is defined by a pair of attachment points, represented by two vectors, $\mathbf{r}_p$ and $\mathbf{r}_c$, in the local reference frames of the parent and the child bones, respectively. We represent the local orientation of the joint by a rotation, $\mathbf{R}_0$, in the local reference frame of the parent. In Section 2.3, we specify how the local orientation

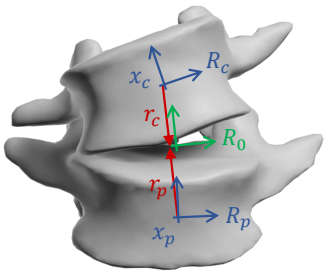

Figure 1: A 6D joint between two vertebrae, showing the rigid configurations of the parent and child vertebrae, $(\mathbf{x}_p, \mathbf{R}_p)$ and $(\mathbf{x}_c, \mathbf{R}_c)$, the attachment points, $\mathbf{r}_p$ and $\mathbf{r}_c$, and the local orientation of the joint, $\mathbf{R}_0$.

of each joint is initialized for an input spine model. We use this local reference frame to decouple the different motion components of the joint, while retaining anisotropic behaviors. Ideally, one would perform personalized motion experiments to understand the possible coupling between motion components [11], and then diagonalize the observed coupled stiffness to obtain a decoupled local reference frame, which enables a simpler model and parameterization of the joint.

Given the attachment points, the local orientation of the joint, and the configurations of the two bones, we can express the translational displacement of the joint as the separation of the attachment points, transformed to the local frame of the joint:

$$\Delta\mathbf{x} = \mathbf{R}_0^T\,\mathbf{R}_p^T\,\left(\mathbf{x}_c + \mathbf{R}_c\,\mathbf{r}_c - \mathbf{x}_p - \mathbf{R}_p\,\mathbf{r}_p\right). \qquad (4)$$

Similarly, we express the rotational displacement of the joint as the separation of the bone orientations, using an angle-axis representation, again transformed to the local frame of the joint:

$$\Delta\theta = \text{ToAxisAngle}\left(\mathbf{R}_0^T\,\mathbf{R}_p^T\,\mathbf{R}_c\,\mathbf{R}_0\right). \qquad (5)$$

Based on the translational and rotational displacements, we set translational and rotational springs. By setting a different stiffness for each DoF of the joint, we achieve an anisotropic behavior, which is crucial for capturing the elastic response of the torso. For each joint, we define $\mathbf{k}_\mathbf{x} = (k_x, k_y, k_z)$, a 3-vector of translational stiffness values, and $\mathbf{k}_\theta = (k_\alpha, k_\beta, k_\gamma)$, a 3-vector of rotational stiffness values. Joint force and torque are naturally formulated as the negative gradients with respect to bone positions and rotations of the following elastic energy:

$$E_i = \frac{1}{2}\,\Delta\mathbf{x}^T\,\text{diag}(\mathbf{k}_x)\,\Delta\mathbf{x} + \frac{1}{2}\,\Delta\theta^T\,\text{diag}(\mathbf{k}_\theta)\,\Delta\theta. \qquad (6)$$

In Section 2.4 below, we discuss the choice of default stiffness values for all joints in the model.

2.3. Articulated-Body Model of the Skeleton

We design an articulated-body model for the skeleton of the torso, focusing on elements that are relevant for predicting the deformation of the lumbar and thoracic spine. To this end, we model the spine including lumbar and thoracic vertebrae, the sternum, the rib cage, and the pelvis, as shown in Fig. 3. We rigidly attach the costal cartilages to the sternum. In Section 2.6 below we describe the boundary conditions applied to the skeleton.

We start with artist-created reference models of the various bones. Given image data of a particular subject in a relaxed standing configuration, we personalize the geometry of the bone models by morphing the reference models to register the image data. To this end, we apply a hierarchical manual deformation, guided by a visual overlay of the deformed model and the input scans. We start with global anisotropic scaling, followed by progressive addition of radial-basis-function 3D deformers [9], and we conclude with anisotropic scaling of individual vertebrae. Fig. 3 shows the skeletal model personalized for two subjects, one with a healthy spine and one suffering from scoliosis.

Once the personalized bones are defined, we proceed by defining the location $\mathbf{r}_p$ and $\mathbf{r}_c$, and local orientation $\mathbf{R}_0$ of joints, for each pair of parent and child vertebrae. There is no consensus in the literature about the placement of the intervertebral joints, especially during lateral bending. Thus, we decided to place the intervertebral joints in the centers of mass of the intervertebral discs, as this choice complies with the main approach in the literature [56]. If the discs are not visible in the subject's images, we place each joint in the middle point between the centers of mass of the two connected vertebrae. We have verified that our results are robust to small changes in joint location. To define the joint orientation $\mathbf{R}_0$ we proceed as follows. We define the Y axis (axial rotation) along the line that connects the centers of mass of the two vertebrae. We then define the X axis (lateral translation in the frontal plane, flexion/extension in the sagittal plane) by fitting a global frontal plane, and finding the axis in the plane that is orthogonal to the Y axis of the joint. Finally, the Z axis (sagittal translation, lateral bending) is computed as the cross-product of the other two.

For the connections between vertebrae and ribs and the ones between ribs and sternum, we place the joints at the midpoint of the closest points between the surfaces of the two connected bones. When searching for the closest point to the sternum, we consider also the rigidly attached costal cartilages. We define the X axis of the joint ('separation' for translation, 'twist' for rotation) by aligning it to the center line of the rib near the joint. Then, we define the Y and Z axes ('alignment' for translation, 'bending' for rotation) arbitrarily in the orthogonal plane, as we use isotropic stiffness values for bending on those axes.

2.4. Joint Stiffness Values

We have defined default stiffness values following the data reported in the study of Ignasiak et al. [27]. While they classify joints based on the number of compliant DoFs (e.g., revolute or spherical), in practice they also model all joints as 6D joints, and report stiffness parameters for stiff DoFs too. Other recent studies also provide experimental

Joint type	$\bar{k}_x$	$\bar{k}_y$	$\bar{k}_z$	$\bar{k}_\alpha$	$\bar{k}_\beta$	$\bar{k}_\gamma$
Thoracic segment	262	1720	262	154	137	154
Lumbar segment	245	1720	245	143	498	149
Rib-vertebrae	53.9	123	123	9.7	6.87	6.87
Rib-sternum	51.85	8	8	9.7	2.29	2.29

Table 1: Default stiffness values (in kN/m for translation, N/rad for rotation) for the various 6D joints in our model, classified into four types.

data for stiffness values, and could be used to modify the default parameters of the model [32, 33, 54].

The intervertebral joints represent the compound effect of intervertebral disks, ligaments, and facet joints. The 6D joints between ribs and vertebrae gather the effect of both the costo-vertebral and costo-transverse joints, which in turn consist of the capsules and the surrounding ligaments. Similarly, the 6D joints between ribs and sternum gather the effect of the costal cartilages and the costo-sternal joints.

In some joints, Ignasiak et al. consider asymmetric stiffness behavior, i.e., different translational stiffness for tension vs. compression (in rib joints), or different rotational stiffness for flexion vs. extension of vertebrae. For simplicity, we have modeled the joints as symmetric, using average stiffness values from the study of Ignasiak et al. The sensitivity analysis we discuss in Section 4.3 supports our choice, as the parameter tolerances cover the asymmetry in the model of Ignasiak et al.

Altogether, we classify four types of joints based on their default stiffness values: thoracic vertebral joints, lumbar vertebral joints, rib-vertebrae joints, and rib-sternum joints. All the default stiffness values are listed in Table 1.

2.5. Soft Tissue

The soft tissue of the torso is composed of multiple and diverse elements, including muscles, organs, and fat. Biomechanical models often focus on the muscles, as they tend to be concerned with the relation between muscle action and the motion of the musculoskeletal system. We are instead concerned with the passive response of the torso to surface forces, and in particular the motion of the spine resulting from this response. Therefore, we ask ourselves what is the overall impact of the soft tissue on this response. Even though the soft tissue of the torso is clearly heterogeneous, we model it as homogeneous on the large scale. As shown in Section 4.3, this will allow us to analyze the overall sensitivity of the soft tissue in contrast to the rest of the parameters of the model. However, it is important to note that soft-tissue parameter tolerances indicate that homogeneity is not a valid assumption for accurate spine deformation.

We start from a 3D scan of the subject's torso, and register it to the rest pose of the skeleton. We mesh the volume of the torso using a Delaunay tetrahedralization of the surface [46]. To attach the soft tissue and the skeletal bones, we sample the bones, and include these samples as constraint nodes for the tetrahedralization. During the simulation, we constrain the motion of these soft-tissue nodes to the corresponding bones.

We have simulated the soft tissue using continuum elasticity equations with FEM discretization [38]. We have tested different options for the choice of material model, and we found that the choice is not critical when analyzing the sensitivity for brace design. Specifically, with a St. Venant-Kirchhoff material and a Neo-Hookean material, the displacements of vertebrae differ by less than 3% under the conditions of our experiments. The principal stretches (eigenvalues of the deformation gradient) range between 0.27 and 1.96, with the largest compressions close to the ribs, but far from the spine, where sensitivity is analyzed.

In the experiments reported in the paper, we have used the Neo-Hookean material. We parameterize the model using Lamé constants, as they avoid artificial sensitivity due to nonlinearity of the material with respect to Poisson's ratio. Using Lamé constants μ (shear modulus) and λ, the Neo-Hookean material is described by the following energy density:

$$\Psi = \frac{\mu}{2}\,(I_1 - 3) - \mu \log J + \frac{\lambda}{2}\,(\log J)^2\,, \qquad (7)$$

where J is the determinant of the deformation gradient $\mathbf{F}$, and I_1 is the first invariant, i.e. the trace, of the right Cauchy-Green tensor $\mathbf{C} = \mathbf{F}^T\mathbf{F}$. We choose default parameter values of 30 kpa for the Young modulus and 0.4 for Poisson's ratio by averaging estimations from multiple references in the literature [10, 26, 35, 47], and we set the corresponding default Lamé constants.

2.6. Boundary Conditions

We distinguish two types of boundary conditions applied to the model: fixed DoFs of the skeleton to provide balance, and external forces that mimic the action of a scoliosis brace. Let us start with how we fix the skeleton.

We wish to simulate postures where the subject remains straight, but allowing some adaptation to the external forces, thus avoiding excessive stress. To this end, we make two choices in how we fix the first thoracic vertebra, T1, and the pelvis. For T1, we fix its lateral and frontal translation, allowing for full rotation and vertical translation, which allow rotation of the spine and the total height to slightly adapt to the external forces. For the pelvis, although most previous works consider it fixed, some exceptions allow it to tilt [13, 37]; therefore, we also allow the pelvis to tilt in our model, and we fix the rest of its DoFs. In practice, we have seen that more restrictive boundary conditions would suffice. We have tested the model with the rotation of T1 fixed, and the displacements of vertebrae differ by less than 17% under our experimental conditions, with little effect on parameter sensitivities. Similarly, we have tested the model with the pelvis fully

fixed, and the displacements of vertebrae differ by less than 8% under our experimental conditions.

We model the action of a brace on the torso and the spine through external forces $\mathbf{f}_{ext}$ applied on the surface of the torso. To determine these forces, we consider the geometry of a brace model and the default parameter values of the torso model, and we simulate the deformation of the torso and the brace with sliding frictional contact between them. Then, we use these same external forces for the rest of our sensitivity study, hence they can be considered fixed. In Section 4.1, we discuss details about the creation of the brace model for our experiments. In early versions of our model, we considered more drastic approximations to brace forces, such as applying forces directly on nearby ribs. We found that the main conclusions about the model and the relative sensitivity of parameters were essentially the same, although modeling the interaction of the brace as a surface force field has revealed higher importance of the flexion/extension stiffness.

2.7. Static Equilibrium

We simulate the deformation of the full torso in reaction to external forces $\mathbf{f}_{ext}$ by solving for static equilibrium configurations, as outlined in Section 2. Let us group in a single vector $\mathbf{x}$ all the DoFs of the torso, consisting of the free FEM nodes of the soft tissue, and the translational and rotational DoFs of the bones. For translation, we use the position of the center of mass of each bone. For orientation, we use the relative rotation with respect to the initial rest configuration, represented using axis angle.

We can formulate the static equilibrium (3) as the minimization of the total energy with respect to the DoFs, i.e.,

$$\mathbf{x} = \arg\min_{\mathbf{x}} \sum_i E_i(\mathbf{x}) + \int_\Omega \Psi(\mathbf{x})\, d\Omega - \mathbf{f}_{ext}^T \mathbf{x}. \qquad (8)$$

Here, we sum the energies E_i of all 6D joints, defined as in (6); the energy density Ψ of the soft tissue, defined as in (7) and integrated over the whole volume Ω of the torso; and the work of external forces $\mathbf{f}_{ext}$. As noted earlier in Section 2.5, we discretize and integrate the soft-tissue energy using tetrahedral FEM.

Note that in our model we do not include gravitational forces. The reason for this is that the input model, obtained from medical images in a standing position, is already pre-loaded with gravitational forces, hence adding gravitational forces to this model would produce wrong deformations. Moreover, the direct effect of brace forces on the deformation of the spine is much larger than the indirect effect due to redistribution of mass, i.e., changes in the gravitational forces. A more accurate approach, which becomes necessary for the correct estimation of stresses in the spine, would be to estimate the rest shape of the spine without gravitational forces, following an optimization approach as done by Clin et al. [14].

3. Methods / Sensitivity Analysis

In this section, we describe how we study the parameterization of the torso model. We are interested in two effects of the parameterization. One is the sensitivity of the different parameters, i.e., which of them have a larger effect on the deformation of the spine under external loads. The other one is the definition of parameter tolerances based on prescribed error bounds on the deformation of the spine. Defining in which range parameters should be in order to ensure accurate spine deformations can serve the design of parameter estimation procedures.

We start this section by providing an overview of our methodology for sensitivity analysis of the parameterization. We leverage tools from differential calculus and linear algebra to derive a sensitivity matrix that relates changes in the parameters to changes in a feature vector. The derivation of the sensitivity matrix requires an implicit solution to static deformations of the spine. By computing a singular value decomposition (SVD) of the sensitivity matrix, we show how to set parameter tolerances based on deformation bounds. We conclude the section by defining a specific feature vector that describes the deformation of the spine, and a reparameterization of the model based on parameter ratios, which is better suited for sensitivity analysis.

3.1. Overview of the Methodology

To analyze the sensitivity of the torso model, we start by defining a feature vector $\mathbf{z}$ that captures relevant information of the geometric state of the model. This feature vector can be evaluated as a function $\mathbf{z}(\mathbf{x})$ of the DoFs of the model. We choose a feature vector that captures positions and rotations of vertebrae, as detailed later in Section 3.3.

In addition to the feature vector, we must define the specific parameter set to be analyzed. The joint stiffness and soft-tissue parameters introduced in Section 2 do not share a common scale, and would complicate a combined sensitivity analysis and the comparison of parameter sensitivities. For sensitivity analysis, we introduce instead a reparameterization of the model based on *parameter ratios*. For each scalar parameter (i.e., a joint stiffness or a Lamé constant in our case), we define its actual value k based on a default value $\bar{k}$ and a ratio ξ_k, such that $k = \xi_k\, \bar{k}$. The parameter vector ξ is then composed of the different parameter ratios. We also group parameter ratios for components of the model with similar biomechanical function, and hence design a compact parameter vector, as detailed later in Section 3.4.

We seek to compute the sensitivity of the feature vector $\mathbf{z}$ with respect to the default model parameters. Under the assumption of small deformations, this sensitivity can be characterized by the Jacobian of the feature vector with respect to the vector of parameter ratios ξ, evaluated at $\xi = 1$ (i.e., with default parameter values). We refer to this Jacobian as the *sensitivity matrix* $\mathbf{S}$.

To compute the sensitivity matrix, we can simply apply the chain rule:

$$\mathbf{S} = \frac{\partial \mathbf{z}}{\partial \xi} = \frac{\partial \mathbf{z}}{\partial \mathbf{x}} \frac{\partial \mathbf{x}}{\partial \xi}. \tag{9}$$

The Jacobian of the feature vector with respect to the DoFs of the torso model, $\frac{\partial \mathbf{z}}{\partial \mathbf{x}}$, is trivial to compute, as it entails only derivatives of rigid transformations with respect to the translations and rotations of vertebrae. On the other hand, the Jacobian of the DoFs with respect to parameter ratios, $\frac{\partial \mathbf{x}}{\partial \xi}$, requires special attention. As the parameters of the torso change, its deformation is defined by the static equilibrium (8). The solution to this problem is given by the static equilibrium condition (3), i.e., zero net forces. By applying the Implicit Function Theorem to this condition, we can obtain the Jacobian of the DoFs with respect to parameter ratios:

$$\mathbf{f}(\mathbf{x}, \xi) + \mathbf{f}_{ext} = 0 \rightarrow \frac{\partial \mathbf{f}}{\partial \mathbf{x}} \frac{\partial \mathbf{x}}{\partial \xi} + \frac{\partial \mathbf{f}}{\partial \xi} = 0 \rightarrow$$
$$\frac{\partial \mathbf{x}}{\partial \xi} = -\frac{\partial \mathbf{f}}{\partial \mathbf{x}}^{-1} \frac{\partial \mathbf{f}}{\partial \xi}. \tag{10}$$

This expression requires the Jacobians of forces with respect to the DoFs, $\frac{\partial \mathbf{f}}{\partial \mathbf{x}}$, and the parameter ratios, $\frac{\partial \mathbf{f}}{\partial \xi}$, which we evaluate analytically.

Under linear approximation, i.e., valid for small changes of parameters, the sensitivity matrix allows exploring the effects of parameters without recomputing torso deformations, which is a costly task. For any parameter change, we can obtain a linear approximation of the resulting deformation. As a corollary, by analyzing the columns of the sensitivity matrix $\mathbf{S}$ and computing their norm, we can sort the parameters according to their sensitivity. In Section 4.3 we perform this operation on several experiments and we discuss the results. However, prior to this, in Section 4.2 we validate the correctness of the linear approximation for sensitivity analysis.

3.2. Model Tolerance Based on SVD

Based on the sensitivity matrix $\mathbf{S}$, a change of parameters $\Delta\xi$ produces a change in the feature vector $\Delta\mathbf{z} = \mathbf{S}\,\Delta\xi$. Given an error bound ϵ on spine deformation (i.e., on the feature vector), we wish to find the largest parameter change $\Delta\xi$, such that the error bound is satisfied, i.e., $\|\Delta\mathbf{z}\| = \|\mathbf{S}\,\Delta\xi\| < \epsilon$.

We propose two approaches to set tolerances on parameters: one with uniform tolerance, the other with sensitivity-based tolerance. Both approaches leverage the SVD of the sensitivity matrix:

$$\mathbf{S} = \mathbf{U}\,\Sigma\,\mathbf{V}^T, \tag{11}$$

with Σ a diagonal matrix of singular values $\{\sigma_j\}$, and $\mathbf{U}$ and $\mathbf{V}$ orthogonal matrices.

Given N_ξ parameters, one can bound the change of the feature vector $\Delta\mathbf{z}$ by bounding uniformly all parameter changes $\{\Delta\xi_k\}$:

$$\|\Delta\xi_k\| < \frac{\epsilon}{\sqrt{N_\xi}\,\sigma_{\max}}, \tag{12}$$

where $\sigma_{\max}$ is the largest singular value. In Appendix A, we include the derivation of this uniform tolerance.

Alternatively, one can bound the change of the feature vector $\Delta\mathbf{z}$ by bounding each parameter change $\Delta\xi_k$ according to sensitivities:

$$\|\Delta\xi_k\| < \frac{\epsilon}{N_\xi \sqrt{\sum_i \sigma_i}\, \max_j \left(\sqrt{\sigma_j}\,\|\mathbf{v}_{k,j}\|\right)}, \tag{13}$$

where $\mathbf{v}_{k,j}$ is the k^{th} component of $\mathbf{v}_j$, a right singular vector of $\mathbf{S}$, i.e., a column of $\mathbf{V}$. In Appendix B, we include the derivation of this sensitivity-based tolerance.

Unlike the uniform tolerance (12), the sensitivity-based tolerance (13) allows the parameter estimation to focus on the most relevant parameters, with loose bounds for insensitive parameters. In Section 4.3, we use these results to set tolerances on the parameters of the torso model according to prescribed bounds on the deformation error.

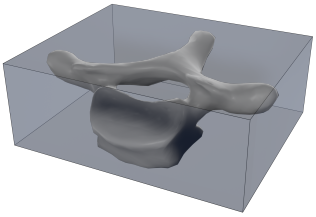

Figure 2: To facilitate the combined analysis of translational and rotational motion of the vertebrae, we place an oriented bounding box around each vertebra, and compute a feature vector consisting of the eight corners of the box.

3.3. Spine Feature Vector

Several metrics exist for the classification and quantification of scoliosis. One popular metric is the Cobb angle [44]. It measures the largest angle between the superior endplate of a vertebra and the inferior endplate of some other vertebra, thus characterizing the maximum bending of the spine. Alternatively, Lenke's classification [30] uses three different spine curves measured between fixed vertebrae. The Cobb angle is not differentiable, and both Cobb angle and Lenke's curves characterize all the deformation of the spine with just one or a few scalar values; therefore, they are not well suited for sensitivity analysis of model parameters. Instead, we design a feature vector that accounts for the deformation of the complete spine, and which is differentiable.

We place an oriented bounding box (OBB) [24] around each vertebra of the spine, as shown in Fig. 2. We build a feature point $\mathbf{z}_i$ using the position of each corner of the OBB, as this feature point accounts for both translation and rotation of the vertebra. By concatenating the feature points of all OBB corners, we obtain the feature vector of

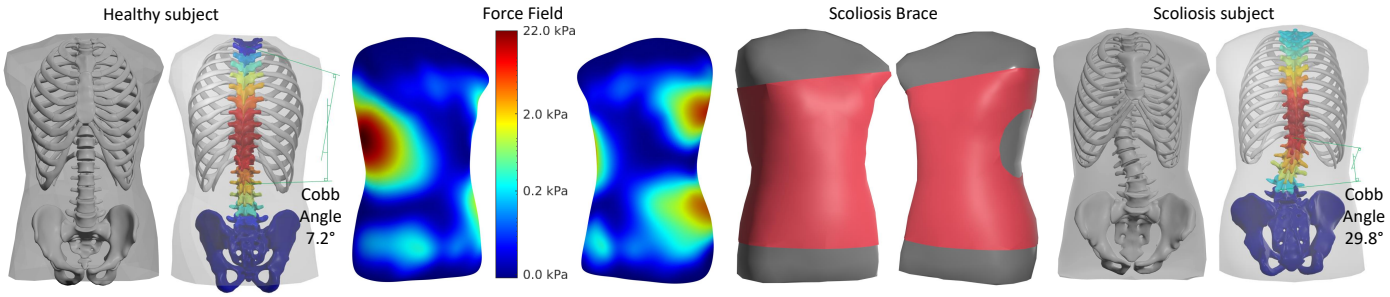

Figure 3: We use two test cases for our study: a reference healthy subject (left) and a subject suffering from scoliosis (right). The grayscale images depict the torso models at rest, with the skeletal elements of our model and the soft-tissue (drawn semitransparent). The color images show the deformation of each vertebra under external forces (blue means no deformation and red means maximum deformation), as well as the resulting Cobb angle. Note that these images are drawn from the back. The center of the figure also shows the surface force field used in the experiments, which was obtained by simulating contact of the scoliosis subject with the pictured brace. The same force field was transferred to the surface of the healthy subject.

the spine, **z**. Note that the feature vector ignores other elements of the model, such as the rib cage, as they do not enter into the computation of the Cobb angle either.

3.4. Parameter Set

With 61 joints, 6 scalar stiffness values per joint, and 2 soft-tissue parameters, brute-force sensitivity analysis would employ a parameter vector with 368 elements. Instead, we assign common parameter ratios to groups of joint stiffness values, and perform sensitivity analysis on a vector ξ of 20 distinct parameter ratios:

- Translation and rotation stiffness of intervertebral joints $\{k_{v,x}, k_{v,y}, k_{v,z}, k_{v,\alpha}, k_{v,\beta}, k_{v,\gamma}\}$.
- Translation and rotation stiffness of rib-vertebrae joints $\{k_{r,x}, k_{r,y}, k_{r,z}, k_{r,\alpha}, k_{r,\beta}, k_{r,\gamma}\}$.
- Translation and rotation stiffness of rib-sternum joints $\{k_{s,x}, k_{s,y}, k_{s,z}, k_{s,\alpha}, k_{s,\beta}, k_{s,\gamma}\}$.
- Lamé constants of the soft tissue, $\{\mu, \lambda\}$.

For simplicity, in the paper we often refer to parameter ratios with the names of their corresponding model parameters. It is important to note that all similar joints share a common parameter ratio for sensitivity analysis, but in the case of lumbar and thoracic vertebrae the default stiffness values are different, as indicated in Table 1. Therefore, a change of, e.g., the axial rotation parameter ratio of intervertebral joints will produce a different actual axial rotation stiffness, $k_{v,\beta}$, for lumbar and thoracic vertebrae.

4. Results

In this section, we discuss the data and conditions of our experiments, the validation of the sensitivity matrix, and conclusions about model parameters obtained by applying sensitivity analysis. In a supplementary document, we provide a comprehensive summary of the experimental results. Here, due to space constraints, we report only the most relevant data. All experiments reported in the study were run using the SOFA simulation framework [2]. The simulation code is written in C++, and SOFA offers a Python interface to easily access simulation and model data.

4.1. Experimental Conditions

Fig. 3 summarizes the data and conditions of our experiments. We have extracted torso models from images of two subjects, following the procedure described in Section 2.3. We refer to these two subjects as *healthy* and *scoliosis* subjects, respectively, in the rest of the document. The healthy subject, shown on the left in Fig. 3 exhibits a Cobb angle of 3.2 degrees at rest, while the scoliosis subject, shown on the right, exhibits a Cobb angle of 31.8 degrees.

In our experiments, we have used boundary conditions that represent the forces exerted by a scoliosis brace, as described in Section 2.6. In particular, we try to mimic the conditions of a 3-point brace applied to the torso of the scoliosis subject. Given the model of the torso of the scoliosis subject, we have designed a model of a brace in the form of a Boston brace [42] (shown in Fig. 3). A 3-point brace applies a lateral force at the height of the main spine curvature, with two opposing forces above and below. Based on this strategy, we have manually modified the geometry of the brace trying to improve the spine deformation, until we reach a total (distributed) load of roughly 250 N on the skin of the torso. This results in a Cobb angle of 29.8 degrees. Fig. 3 also shows the resulting pressure distribution on the skin. Many studies tried to estimate the forces exerted by a scoliosis brace on the patient, using pressure sensors [1, 12, 34, 49]. These studies report force values in the range from 100 to 600 N. We chose to apply a force of 250 N, as an approximate average of the reported values.

As discussed in Section 2.6, we compute the brace force using a full simulation of contact between the brace and the torso, but we then fix these external forces for sensitivity analysis. For the healthy subject, we define a correspondence mapping to the skin of the scoliosis subject,

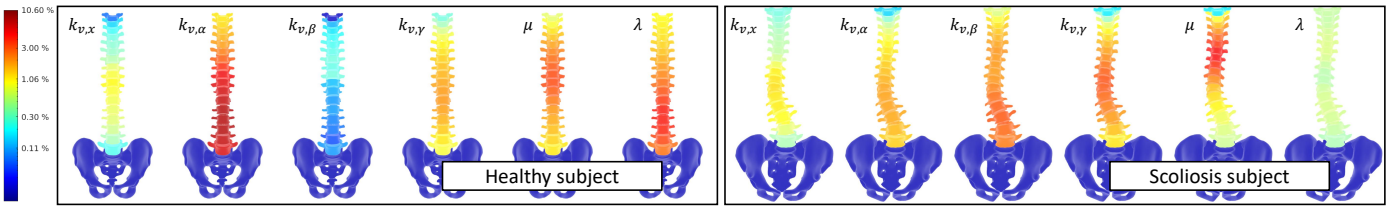

Figure 4: Validation of the sensitivity matrix. The images illustrate, for both subjects and the test conditions indicated in Fig. 3, the error (in logarithmic scale) between deformations estimated using the sensitivity matrix vs. deformations computed by solving full static equilibrium problems. The images show errors resulting from a 10% change of individual parameters, computed for each vertebra independently, and normalized with respect to the largest vertebra displacement. We depict only the parameters with highest sensitivity.

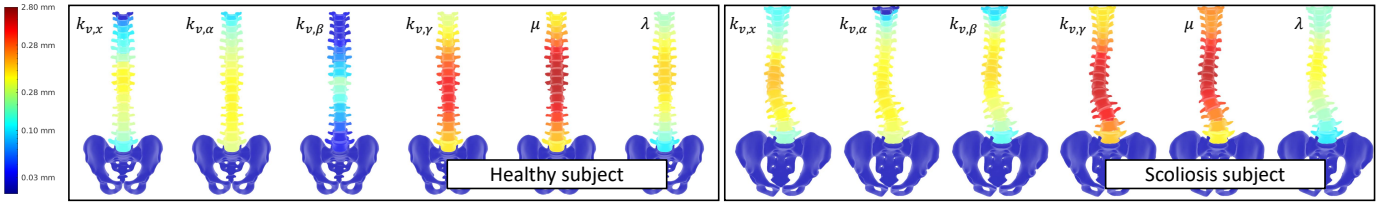

Figure 5: Sensitivity of the parameters of the torso model. The images illustrate, for both subjects and the test conditions depicted in Fig. 3, the displacement of vertebrae (in logarithmic scale) corresponding to a 100% change of individual parameters. We depict only the most sensitive parameters.

and we use this mapping to transfer the same brace forces. Of course, on the healthy subject these forces produce a negative effect and increase the Cobb angle to 7.2 degrees.

4.2. Validation of the Sensitivity Matrix

As discussed in Section 3, the sensitivity matrix $\mathbf{S}$ provides a linear approximation of the deformation due to changes in parameters. Before carrying out sensitivity analysis of the model parameters using the sensitivity matrix, we validate its accuracy. We do this by comparing the deformation predicted through the sensitivity matrix $\mathbf{S}$, with the actual change of deformation, on both the healthy and scoliosis subjects.

We have tested changes of 1% and 10% to all parameters, i.e., values of parameter ratios of 1.01 and 1.1 respectively. Fig. 4 summarizes the error induced by the sensitivity matrix for the six most relevant parameters, for parameter changes of 10%. Errors for the rest of the parameters are negligible. In the figure, we depict the relative RMS error of the feature vector of each vertebra, normalized by the largest RMS feature vector among all vertebrae.

We can conclude that the sensitivity matrix is accurate, as the maximum error for a parameter change of 10% is less than 10% of the maximum displacement. We also identify six parameters that produce larger error, roughly in this order for the scoliosis subject: shear modulus μ, intervertebral axial rotation stiffness $k_{v,\beta}$, intervertebral lateral bending stiffness $k_{v,\gamma}$, intervertebral flexion/extension stiffness $k_{v,\alpha}$, intervertebral lateral translation stiffness $k_{v,x}$, and Lamé's parameter λ. For the healthy subject, the error is distributed differently, as shown in Fig. 4.

From an analysis of the error, we can also observe that larger error is present at the lower thoracic and upper lumbar part. This is no surprise, as this is the region where the lateral force is acting.

4.3. Sensitivity Analysis

The sensitivity matrix allows us to compare sensitivity of the deformation to the various parameters, and hence understand which parameters, and in what combinations, require tighter tolerance for accurate prediction of deformations. We start by evaluating sensitivity with respect to individual parameters. This boils down to analyzing the columns in $\mathbf{S}$ separately. Fig. 5 illustrates the change in deformation of the spine produced by a 100% change in each parameter, for both subjects shown in Fig. 3. The images are color-coded per vertebra, based on the RMS of the feature vector of each vertebra. They display deformations for the six dominant parameters, roughly in this order: shear modulus μ, intervertebral lateral bending stiffness $k_{v,\gamma}$, intervertebral lateral translation stiffness $k_{v,x}$, intervertebral axial rotation stiffness $k_{v,\beta}$, intervertebral flexion/extension stiffness $k_{v,\alpha}$, and Lamé's parameter λ. A comparison between the scoliosis and healthy subjects reveals slightly higher sensitivity for the scoliosis subject. The difference is most notable for the intervertebral axial rotation stiffness $k_{v,\beta}$, which is not sensitive at all in the case of the healthy subject.

Fig. 6 presents the four first right singular vectors for both subjects, following the mathematical derivation described in Section 3.2. The singular vectors are scaled by their corresponding singular value, and divided by $\sqrt{144}$, where 144 is the number of vertebra corners, to indicate RMS magnitudes per corner. From the combination of results in Fig. 5 and Fig. 6 we can draw some conclusions. Soft-tissue parameters, intervertebral lateral stiff-

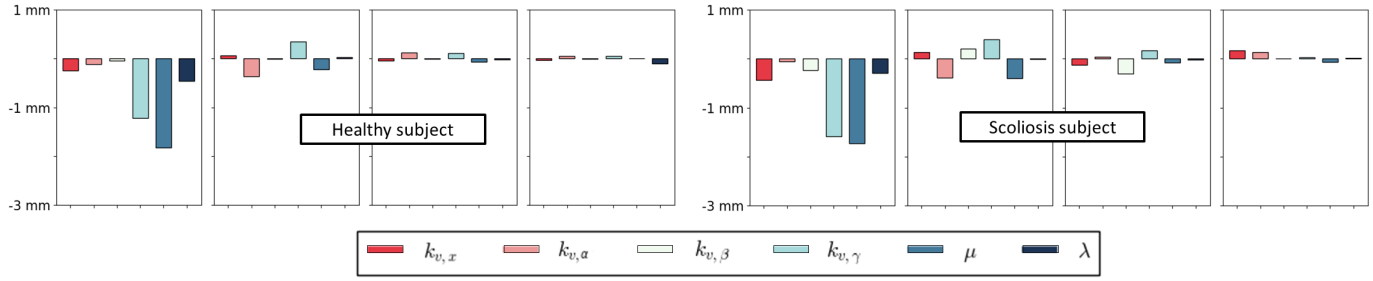

Figure 6: Eigenanalysis of sensitivity. The bar plots illustrate, for both subjects depicted in Fig. 3, the four main right singular vectors of the sensitivity matrix, scaled by their corresponding singular values and normalized to indicate RMS values per feature point (i.e., vertebra OBB corner). We depict only the vector components corresponding to the most sensitive parameters.

Parameters	All	$k_{v,x}$	$k_{v,y}$	$k_{v,z}$	$k_{v,\alpha}$	$k_{v,\beta}$	$k_{v,\gamma}$	$k_{r,x}$	$k_{r,y}$	$k_{r,z}$	$k_{r,\alpha}$	$k_{r,\beta}$	$k_{r,\gamma}$	$k_{s,x}$	$k_{s,y}$	$k_{s,z}$	$k_{s,\alpha}$	$k_{s,\beta}$	$k_{s,\gamma}$	μ	λ
Tol. (%), 5 mm max.	26	20	42	77	17	14	7	380	709	892	131	290	26	638	200	136	274	2464	256	7	36
Tol. (%), 5 mm RMSE	46	35	61	74	26	24	11	131	446	363	128	135	53	340	134	192	284	486	236	10	39

Table 2: Tolerances (in percentage) for all parameters in the model, to guarantee an error bound of 5 mm in spine deformation. We compute tolerances in two ways: uniform tolerance (12) (column 'All'), and sensitivity-based per-parameter tolerance (13) (rest of the columns). We also enforce bounds in two ways: a maximum error of 5 mm among vertebra OBB corners, and an RMSE of 5 mm across corners.

ness (both translation and rotation), intervertebral axial rotation stiffness, and intervertebral flexion/extension stiffness are clearly the parameters that require careful estimation for accurate model prediction. Moreover, the intervertebral parameters gain relevance for scoliosis subjects, but the correct estimation of soft-tissue parameters cannot be neglected. Intervertebral axial rotation stiffness is hardly relevant for healthy subjects, but it gains importance for scoliosis subjects. This conclusion matches expectations, as scoliosis subjects tend to suffer some axial rotation of the spine in their rest configuration.

Lastly, we have derived tolerances for model parameters, following the mathematical derivation in Section 3.2. In Table 2, we report both uniform tolerance (12) and sensitivity-based tolerance (13) for the model parameters, for an error bound of 5 mm. We report tolerances only for the scoliosis subject. We apply the 5 mm error bound in two different ways. First, we consider an absolute bound on all vertebra corners. To this end, we study separately the sensitivity matrix $\mathbf{S}_i$ of the feature point $\mathbf{z}_i$ of each corner, and we retain the tightest tolerance for each parameter. Second, we consider an RMS error of 5 mm on the complete spine, and we study the complete sensitivity matrix $\mathbf{S}$. With 144 vertebra corners, this amounts to an error bound of $\epsilon = \sqrt{144} \times 5$ mm $= 6$ cm for the expressions in Section 3.2.

For an absolute bound of 5 mm per vertebra corner, the uniform parameter tolerance is 26%. With sensitivity-based tolerance, only five parameters (highlighted in the table) require a tighter tolerance (in this order: intervertebral lateral bending stiffness $k_{v,\gamma}$, shear modulus μ, intervertebral axial rotation stiffness $k_{v,\beta}$, intervertebral flexion/extension stiffness $k_{v,\alpha}$, intervertebral lateral translation stiffness $k_{v,x}$). For all other parameters, sensitivity-based tolerances are relaxed. Some tolerances are so wide that they exit the linear regime. Those values cannot be taken literally; they represent that the tolerances allowed are very large. But it is possible to draw some important conclusions. The wide tolerances validate several of our model design choices, such as the approximations in rib joints and cartilages. We also pay particular attention to the parameterization of the intervertebral flexion/extension stiffness $k_{v,\alpha}$. Previous work used asymmetric stiffness for this rotation (with a deviation of 17% with respect to the average value) [27]. Our analysis validates that, under the loading conditions we studied, a choice of symmetric stiffness is sufficient for an error bound of 5 mm, as the parameter tolerance is precisely 17%. However, asymmetric stiffness would be required to enforce a tighter error bound and/or different loading conditions.

5. Discussion

This work describes the development of a comprehensive model of torso and spine biomechanics, together with computational tools that enable sensitivity analysis of the model and its parameters. This analysis sets guidelines for the parameter estimation of personalized torso and spine models in the context of computational design of scoliosis braces.

From the analysis, we draw the following main conclusions. Not surprisingly, the intervertebral lateral stiffness (both translation and rotation) is one of the factors that requires careful modeling. But perhaps more surprisingly, the shear modulus of the soft tissue in the torso requires equal care. For subjects suffering from scoliosis, but not for healthy subjects, intervertebral axial rotation stiffness must be carefully modeled too. For moderate accuracy,

all other mechanical parameters of the torso model can be largely approximated. In particular, complex anatomical elements such as rib joints can use simple approximate models. Even the intervertebral flexion/extension stiffness, which in other works is considered asymmetric to distinguish flexion and extension, can be approximated unless high accuracy is needed.

The study described in the paper could be further extended to understand additional factors. In the experiments, brace forces were kept constant during sensitivity analysis, and minor adaptations of these forces were ignored. The soft tissue of the torso was modeled as homogeneous, and the possible effects of material heterogeneity remain unclear. One of such effects could be errors on the strain and stress distributions, even if the overall positions are similar. Similarly, large segments of the spine were modeled as homogeneous, but local changes of intervertebral stiffness are known to occur in reality, both due to deformities such as scoliosis itself, or simply because more deformed areas tend to be stiffer. Nevertheless, note that our model is not personalized; therefore, the stiffness values can be considered default parameters. For a personalized model, the parameters for each joint should be different and they should meet the tolerances indicated by the sensitivity analysis. All experiments were carried out ignoring muscle forces, under one of two possible assumptions, that the average force over time is negligible, or that scoliosis braces produce most of their effect through periods of little muscle activity. It would be interesting to extend the study with a model of muscle activity, a larger body model to include full handling of the pelvis and the cervical region, and motion of the body in various postures. The study was executed on spine data sets of a subject suffering from scoliosis and a healthy subject, but the range of scoliosis types is large. The study could be extended by analyzing sensitivity on data sets corresponding, for example, to different types within Lenke's classification [30].

The proposed methodology for sensitivity analysis is not restricted to the torso model presented in this paper. The methodology is general, and could be applied to other models, with different components and/or different design choices. In this regard, it is important to design parameterizations which balance appropriately the relevance of different model components and their parameters. To this end, we parameterize our model using parameter ratios over default parameter values, and we group parameter ratios of multiple model components. Our approach could be generalized by normalizing parameters based on some objective metric, such as their contribution to the system energy.

We started this work as part of a broader project, concerned with the development of personalized brace design tools for adolescent idiopathic scoliosis. In the design of such tools, we encountered unknowns about the model choices, but most importantly we encountered many unknowns about the required accuracy in the parameterization. To address these unknowns, we developed and applied the methodology for sensitivity analysis presented in this paper. Thanks to the conclusions of the paper, we have developed a methodology for personalized parameter estimation, and we are currently applying this methodology to a cohort of scoliosis patients. This continuation study will allow us to evaluate the accuracy of the personalized models, and will also provide data to estimate better default parameter values.

Finally, even though the tools developed in this work are general, the conditions of the study and the conclusions are particular to the analysis of the effect of scoliosis braces. The tools and the analysis could be generalized to other applications of biomechanical models of the torso, such as posture or gait analysis, or even to biomechanical models of other parts of the body.

Funding

This project has received funding from the European Union's Horizon 2020 research and innovation programme under the Marie Sklodowska-Curie grant agreement No. 764644, Rainbow. This paper only contains the author's views and the Research Executive Agency and the Commission are not responsible for any use that may be made of the information it contains.

Acknowledgements

The authors would like to thank the team members of AnatoScope SA Francois Faure, Matthieu Nesme, Thomas Lemaire, Ulysee Vimont, Nicolas Comte, Elie Cattan, Vincent Luboz and Maxime Tournier for their valuable contribution in the simulation software, the provision of the subjects' geometry and the fruitful discussions about the mechanical concept. Furthermore, they would like to thank Hamed Shayestehpour and Faezeh Moshfeghifar for their valuable contribution in the conception of the biomechanical model and Cristian Romero for his priceless help in the visualization of the results.

Ethical approval

All data used in this paper was provided, already anonymized, by AnatoScope SA. Data acquisition was carried out after ethical clearance. No other aspect of this work triggered ethical issues.

Declaration of Competing Interests

The authors declare that they have no known competing financial interests or personal relationships that could have appeared to influence the work reported in this paper.

References

[1] Asliza Ahmad, Noor Azuan Abu Osman, Halim Mokhtar, Waqas Mehmood, and Nahrizul Adib Kadri. Analysis of the interface pressure exerted by the chêneau brace in patients with double-curve adolescent idiopathic scoliosis. *Proceedings of the Institution of Mechanical Engineers, Part H: Journal of Engineering in Medicine*, 233(9):901–908, 2019.

[2] Jérémie Allard, Stéphane Cotin, François Faure, Pierre-Jean Bensoussan, François Poyer, Christian Duriez, Hervé Delingette, and Laurent Grisoni. SOFA - an Open Source Framework for Medical Simulation. In *MMVR 15 - Medicine Meets Virtual Reality*, volume 125 of *Studies in Health Technology and Informatics*, pages 13–18, Palm Beach, United States, 2007. IOP Press.

[3] Rozilene Maria C Aroeira, Antônio Eustáquio M Pertence, Daniel Takanori Kemmoku, and Marcelo Greco. The effect of hypokyphosis on the biomechanical behavior of the adolescent thoracic spine. *Journal of the Brazilian Society of Mechanical Sciences and Engineering*, 40(3):128, 2018.

[4] Rozilene Maria Cota Aroeira, Antônio Eustáquio de Melo Pertence, Daniel Takanori Kemmoku, and Marcelo Greco. Three-dimensional geometric model of the middle segment of the thoracic spine based on graphical images for finite element analysis. *Research on Biomedical Engineering*, 33(2):97–104, 2017.

[5] Sabine Bauer, Eva Keller, and Dietrich Paulus. Sensitivity analysis of intervertebral disc parameters: Mbs model of the lumbar spine. *International Journal of Engineering and Applied Sciences*, 3(5), 2016.

[6] Riza Bayoglu, Pavel E Galibarov, Nico Verdonschot, Bart Koopman, and Jasper Homminga. Twente spine model: A thorough investigation of the spinal loads in a complete and coherent musculoskeletal model of the human spine. *Medical engineering & physics*, 68:35–45, 2019.

[7] Riza Bayoglu, Ogulcan Guldeniz, Nico Verdonschot, Bart Koopman, and Jasper Homminga. Sensitivity of muscle and intervertebral disc force computations to variations in muscle attachment sites. *Computer methods in biomechanics and biomedical engineering*, 22(14):1135–1143, 2019.

[8] Arno Bisschop, Margriet G. Mullender, Idsart Kingma, Timothy U. Jiya, Albert J. van der Veen, Jan C. Roos, Jaap H. van Dieën, and Barend J. van Royen. The impact of bone mineral density and disc degeneration on shear strength and stiffness of the lumbar spine following laminectomy. *European Spine Journal*, 2012.

[9] Mario Botsch and Leif Kobbelt. Real-Time Shape Editing using Radial Basis Functions. *Computer Graphics Forum*, 24(3), 2005.

[10] APC Choi and YP Zheng. Estimation of young's modulus and poisson's ratio of soft tissue from indentation using two different-sized indentors: finite element analysis of the finite deformation effect. *Medical and Biological Engineering and Computing*, 43(2):258–264, 2005.

[11] J. Cholewicki, J. Crisco, T. Oxland, I. Yamamoto, and M. Panjabi. Effects of posture and structure on three-dimensional coupled rotations in the lumbar spine: A biomechanical analysis. *Spine*, 21:2421–2428, 1996.

[12] Chloe L Chung, Derek M Kelly, Jeffery R Sawyer, Jack R Steele, Terry S Tate, Cody K Bateman, and Denis J DiAngelo. Mechanical testing of a novel fastening device to improve scoliosis bracing biomechanics for treating adolescent idiopathic scoliosis. *Applied bionics and biomechanics*, 2018, 2018.

[13] Julien Clin, Carl-Eric Aubin, and Hubert Labelle. Virtual prototyping of a brace design for the correction of scoliotic deformities. *Medical & Biological Engineering & Computing*, 45(5):467–473, 2007.

[14] Julien Clin, Carl-Éric Aubin, Nadine Lalonde, Stefan Parent, and Hubert Labelle. A new method to include the gravitational forces in a finite element model of the scoliotic spine. *Medical & biological engineering & computing*, 49(8):967–977, 2011.

[15] Julien Clin, Carl-Eric Aubin, Stefan Parent, Archana Sangole, and Hubert Labelle. Comparison of the biomechanical 3d efficiency of different brace designs for the treatment of scoliosis using a finite element model. *European Spine Journal*, 19(7):1169–1178, 2010.

[16] N. Cobetto, C. E. Aubin, S. Parent, J. Clin, S. Barchi, I. Turgeon, and Hubert Labelle. Effectiveness of braces designed using computer-aided design and manufacturing (CAD/CAM) and finite element simulation compared to CAD/CAM only for the conservative treatment of adolescent idiopathic scoliosis: a prospective randomized controlled trial. *European Spine Journal*, 25:3056–3064, 2016.

[17] Nikita Cobetto, Carl-Éric Aubin, Stefan Parent, Soraya Barchi, Isabelle Turgeon, and Hubert Labelle. 3d correction of ais in braces designed using cad/cam and fem: a randomized controlled trial. *Scoliosis and spinal disorders*, 12(1):1–8, 2017.

[18] Mark de Zee, Lone Hansen, Christian Wong, John Rasmussen, and Erik B. Simonsen. A generic detailed rigid-body lumbar spine model. *Journal of Biomechanics*, 40:1219–1227, 2007.

[19] Ali Hamadi Dicko, Nicolas Tong-Yette, Benjamin Gilles, François Faure, and Olivier Palombi. Construction and validation of a hybrid lumbar spine model for the fast evaluation of intradiscal pressure and mobility. *World Academy of Science, Engineering and Technology*, 2015.

[20] Enchun Dong, Lei Shi, Jianfeng Kang, Dichen Li, Bin Liu, Zheng Guo, Ling Wang, and Xiangdong Li. Biomechanical characterization of vertebral body replacement in situ: Effects of different fixation strategies. *Computer Methods and Programs in Biomedicine*, page 105741, 2020.

[21] Hakan Ersoy and Ata Muğan. Design sensitivity analysis of structures based upon the singular value decomposition. *Computer Methods in Applied Mechanics and Engineering*, 191(32):3459 – 3476, 2002.

[22] Sean M Finley, Darrel S Brodke, Nicholas T Spina, Christine A DeDen, and Benjamin J Ellis. Febio finite element models of the human lumbar spine. *Computer methods in biomechanics and biomedical engineering*, 21(6):444–452, 2018.

[23] D Gignac, C-É Aubin, J Dansereau, and H Labelle. Optimization method for 3d bracing correction of scoliosis using a finite element model. *European spine journal*, 9(3):185–190, 2000.

[24] S. Gottschalk, M. C. Lin, and D. Manocha. Obbtree: A hierarchical structure for rapid interference detection. In *Proceedings of the 23rd Annual Conference on Computer Graphics and Interactive Techniques*, SIGGRAPH '96, page 171–180, New York, NY, USA, 1996. Association for Computing Machinery.

[25] Aymeric Guy, Hubert Labelle, Soraya Barchi, Elisabeth Audet-Duchesne, Nikita Cobetto, Stefan Parent, Maxime Raison, and Carl-Éric Aubin. Braces designed using cad/cam combined or not with finite element modeling lead to effective treatment and quality of life after 2 years: A randomized controlled trial. *Spine*, 46(1):9–16, 2021.

[26] Alexandre Hostettler, Daniel George, Yves Rémond, Stéphane André Nicolau, Luc Soler, and Jacques Marescaux. Bulk modulus and volume variation measurement of the liver and the kidneys in vivo using abdominal kinetics during free breathing. *Computer methods and programs in biomedicine*, 100(2):149–157, 2010.

[27] Dominika Ignasiak, Sebastian Dendorfer, and Stephen J. Ferguson. Thoracolumbar spine model with articulated rib cage for the prediction of dynamic spinal loading. *Journal of Biomechanics*, 2015.

[28] Timothy L Lasswell, Duane S Cronin, John B Medley, and Parham Rasoulinejad. Incorporating ligament laxity in a finite element model for the upper cervical spine. *The Spine Journal*, 17(11):1755–1764, 2017.

[29] Franck Le Navéaux, A Noelle Larson, Hubert Labelle, Xiaoyu Wang, and Carl-Éric Aubin. How does implant distribution affect 3d correction and bone-screw forces in thoracic adolescent idiopathic scoliosis spinal instrumentation? *Clinical Biomechanics*, 39:25–31, 2016.

[30] Lawrence G. Lenke, Randal R. Betz, Jürgen Harms, Keith H. Bridwell, David H. Clements, Thomas G. Lowe, and Kathy

Blanke. Adolescent idiopathic scoliosis: A new classification to determine extent of spinal arthrodesis. *The Journal of Bone & Joint Surgery*, 83(8):1169–1181, 2001.
[31] Yi-Ching Liao, Chi-Kuang Feng, Mei-Wun Tsai, Chen-Sheng Chen, Cheng-Kung Cheng, and Yu-Chih Ou. Shape modification of the boston brace using a finite-element method with topology optimization. *Spine*, 32(26):3014–3019, 2007.
[32] Christian Liebsch, Nicolas Graf, Konrad Appelt, and Hans-Joachim Wilke. The rib cage stabilizes the human thoracic spine: An in vitro study using stepwise reduction of rib cage structures. *PLoS One*, 12(6):e0178733, 2017.
[33] Christian Liebsch, Nicolas Graf, and Hans-Joachim Wilke. In vitro analysis of kinematics and elastostatics of the human rib cage during thoracic spinal movement for the validation of numerical models. *Journal of biomechanics*, 94:147–157, 2019.
[34] Ioannis Loukos, Constantinos Zachariou, Christos Nicolopoulos, Dimitrios Korres, and Nicolaos Efstathopoulos. Analysis of the corrective forces exerted by a dynamic derotation brace (ddb). *Prosthetics and orthotics international*, 35(4):365–372, 2011.
[35] Clayton T McKee, Julie A Last, Paul Russell, and Christopher J Murphy. Indentation versus tensile measurements of young's modulus for soft biological tissues. *Tissue Engineering Part B: Reviews*, 17(3):155–164, 2011.
[36] Sean P Moroney, Albert B Schultz, James AA Miller, and Gunnar BJ Andersson. Load-displacement properties of lower cervical spine motion segments. *Journal of biomechanics*, 21(9):769–779, 1988.
[37] Wen-Zhong Nie, Ming Ye, Zu-De Liu, and Cheng-Tao Wang. The patient-specific brace design and biomechanical analysis of adolescent idiopathic scoliosis. *Journal of biomechanical engineering*, 131(4), 2009.
[38] R.W. Ogden. *Non-linear Elastic Deformations*. Dover Publications, 1997.
[39] Manohar M Panjabi, Richard A Brand Jr, and Augustus A White III. Three-dimensional flexibility and stiffness properties of the human thoracic spine. *Journal of biomechanics*, 9(4):185–192, 1976.
[40] Manohar M Panjabi, TR Oxland, I Yamamoto, and Joseph J Crisco. Mechanical behavior of the human lumbar and lumbosacral spine as shown by three-dimensional load-displacement curves. *The Journal of bone and joint surgery. American volume*, 76(3):413–424, 1994.
[41] Michael Putzer, Ingo Ehrlich, John Rasmussen, Norbert Gebbeken, and Sebastian Dendorfer. Sensitivity of lumbar spine loading to anatomical parameters. *Journal of biomechanics*, 49(6):953–958, 2016.
[42] D Périé, CE Aubin, Y Petit, M Beauséjour, J Dansereau, and H Labelle. Boston brace correction in idiopathic scoliosis: a biomechanical study. *Spine*, 28(15):1672–1677, 2003.
[43] Margaret E Raabe and Ajit MW Chaudhari. An investigation of jogging biomechanics using the full-body lumbar spine model: Model development and validation. *Journal of biomechanics*, 49(7):1238–1243, 2016.
[44] A Safari, H Parsaei, A Zamani, and B Pourabbas. A semi-automatic algorithm for estimating cobb angle. *Journal of Biomedical Physics & Engineering*, 9(3):317, 2019.
[45] Marco Senteler, Ameet Aiyangar, Bernhard Weisse, Mazda Farshad, and Jess G Snedeker. Sensitivity of intervertebral joint forces to center of rotation location and trends along its migration path. *Journal of biomechanics*, 70:140–148, 2018.
[46] Jonathan Richard Shewchuk. Tetrahedral mesh generation by delaunay refinement. In *Proceedings of the fourteenth annual symposium on Computational geometry*, pages 86–95, 1998.
[47] Chengli Song, Afshin Alijani, Tim Frank, George Hanna, and Alfred Cuschieri. Elasticity of the living abdominal wall in laparoscopic surgery. *Journal of biomechanics*, 39(3):587–591, 2006.
[48] Andriacchi T, Schultz A, Belytschko T, and Galante J. A model for studies of mechanical interactions between the human spine and rib cage. *Journal of Biomechanics*, 7:497–507, 1974.
[49] JAAM Van den Hout, L Van Rhijn, R Van den Munckhof, and A Van Ooy. Interface corrective force measurements in boston brace treatment. *European Spine Journal*, 11(4):332–335, 2002.
[50] F. van Keulen, R.T. Haftka, and N.H. Kim. Review of options for structural design sensitivity analysis. part 1: Linear systems. *Computer Methods in Applied Mechanics and Engineering*, 194(30):3213 – 3243, 2005.
[51] Claudio Vergari, Zhuowei Chen, Léopold Robichon, Isabelle Courtois, Eric Ebermeyer, Raphaël Vialle, Tristan Langlais, Raphaël Pietton, and Wafa Skalli. Towards a predictive simulation of brace action in adolescent idiopathic scoliosis. *Computer Methods in Biomechanics and Biomedical Engineering*, pages 1–8, 2020.
[52] Claudio Vergari, Isabelle Courtois, Eric Ebermeyer, Houssam Bouloussa, Raphaël Vialle, and Wafa Skalli. Experimental validation of a patient-specific model of orthotic action in adolescent idiopathic scoliosis. *European Spine Journal*, 25(10):3049–3055, 2016.
[53] Wenhai Wang, George R Baran, Randal R Betz, Amer F Samdani, Joshua M Pahys, and Patrick J Cahill. The use of finite element models to assist understanding and treatment for scoliosis: a review paper. *Spine Deformity*, 2(1):10–27, 2014.
[54] Hans-Joachim Wilke, Andrea Herkommer, Karin Werner, and Christian Liebsch. In vitro analysis of the segmental flexibility of the thoracic spine. *PLoS One*, 12(5):e0177823, 2017.
[55] Ming Xu, James Yang, Isador H Lieberman, and Ram Haddas. Lumbar spine finite element model for healthy subjects: development and validation. *Computer methods in biomechanics and biomedical engineering*, 20(1):1–15, 2017.
[56] Thomas Zander, Marcel Dreischarf, and Hendrik Schmidt. Sensitivity analysis of the position of the intervertebral centres of reaction in upright standing–a musculoskeletal model investigation of the lumbar spine. *Medical engineering & physics*, 38(3):297–301, 2016.

Appendix A. Uniform Tolerance

We wish to find the largest parameter change $\|\Delta\xi\|$ such that the resulting change of feature vector $\|\Delta\mathbf{z}\|$ satisfies an error bound ϵ, i.e.,

$$\epsilon > \|\Delta\mathbf{z}\| = \|\mathbf{S}\,\Delta\xi\|. \tag{A.1}$$

For any parameter change, the resulting change of the feature vector can be bounded based on the largest singular value $\sigma_{\max}$ by $\|\mathbf{S}\,\Delta\xi\| < \sigma_{\max}\,\|\Delta\xi\|$. Then, the bound (A.1) is satisfied if

$$\epsilon > \sigma_{\max}\,\|\Delta\xi\| \Rightarrow \|\Delta\xi\| < \frac{\epsilon}{\sigma_{\max}}. \tag{A.2}$$

Given N_ξ parameters, one can bound the norm $\|\Delta\xi\|$ by bounding uniformly all parameter changes $\{\Delta\xi_k\}$, which yields the uniform tolerance:

$$\|\Delta\xi_k\| < \frac{\epsilon}{\sqrt{N_\xi}\,\sigma_{\max}}. \tag{A.3}$$

Appendix B. Sensitivity-Based Tolerance

Alternatively, one can square the bound (A.1), and substitute the SVD (11) to relate the parameter change to the error bound as:

$$\epsilon^2 > \Delta\xi^T\,\mathbf{S}^T\,\mathbf{S}\,\Delta\xi = \sum_j \sigma_j^2\,(\mathbf{v}_j^T\,\Delta\xi)^2, \tag{B.1}$$

where the summation runs over all singular values $\{\sigma_j\}$ and corresponding right singular vectors $\{\mathbf{v}_j\}$ of $\mathbf{S}$.

In this summation, one can bound each addend by a fraction of the bound proportional to the corresponding singular value, i.e.,

$$\begin{aligned} \sigma_j^2 \left(\mathbf{v}_j^T \, \Delta\xi\right)^2 < \frac{\sigma_j \, \epsilon^2}{\sum_i \sigma_i}, \forall j \Rightarrow \\ \sqrt{\sigma_j} \left\|\mathbf{v}_j^T \, \Delta\xi\right\| < \frac{\epsilon}{\sqrt{\sum_i \sigma_i}}, \forall j. \end{aligned} \tag{B.2}$$

Given N_ξ parameters, one can bound the dot product $\mathbf{v}_j^T \, \Delta\xi$ by bounding each addend by a fraction $\frac{1}{N_\xi}$ of the total bound:

$$\sqrt{\sigma_j} \left\|\mathbf{v}_{k,j}\right\| \left\|\Delta\xi_k\right\| < \frac{\epsilon}{N_\xi \sqrt{\sum_i \sigma_i}}, \forall j. \tag{B.3}$$

By choosing the singular value that produces the largest weight $\sqrt{\sigma_j} \left\|\mathbf{v}_{k,j}\right\|$, we obtain the sensitivity-based tolerance:

$$\left\|\Delta\xi_k\right\| < \frac{\epsilon}{N_\xi \sqrt{\sum_i \sigma_i} \, \max_j \left(\sqrt{\sigma_j} \left\|\mathbf{v}_{k,j}\right\|\right)}. \tag{B.4}$$